Icarus 220 (2012) 254–267

Contents lists available at SciVerse ScienceDirect

Icarus

journal homepage: www.elsevier.com/locate/icarus

Problems determining relative and absolute ages using the small crater population

Zhiyong Xiao [a,b,*], Robert G. Strom [b]

[a] Faculty of Earth Sciences, China University of Geosciences (Wuhan), Wuhan, Hubei Province 430074, China
[b] Lunar and Planetary Laboratory, University of Arizona, Tucson, AZ 85721, USA

ARTICLE INFO

Article history:
Received 23 June 2011
Revised 3 May 2012
Accepted 8 May 2012
Available online 17 May 2012

Keywords:
Moon
Mars
Cratering
Geological processes
Impact processes

ABSTRACT

The small crater populations (diameter smaller than 1 km) are widely used to date planetary surfaces. The reliability of small crater counts is tested by counting small craters at several young and old lunar surfaces, including Mare Nubium and craters Alphonsus, Tycho and Giordano Bruno. Based on high-resolution images from both the Lunar Reconnaissance Orbiter Camera and Kaguya Terrain Camera, small craters in two different diameter ranges are counted for each counting area. Large discrepancies exist in both the cumulative (absolute model ages) and relative plots for the two different size ranges of the same counting areas. The results indicate that dating planetary surfaces using small crater populations is highly unreliable because the contamination of secondaries may invalidate the results of small crater counts. A comparison of the size–frequency distributions of the small crater populations and impact ejected boulders around fresh lunar craters shows the same upturn as typical martian secondaries, which supports the argument that secondaries dominate the small crater populations on the Moon and Mars. Also, the size–frequency distributions of small rayed lunar and martian craters of probable primary origin are similar to that of the Population 2 craters on the inner Solar System bodies post-dating Late Heavy Bombardment. Dating planetary surfaces using the small crater populations requires the separation of primaries from secondaries which is extremely difficult. The results also show that other factors, such as different target properties and the subjective identification of impact craters by different crater counters, may also affect crater counting results. We suggest that dating planetary surfaces using small crater populations should be with highly cautious.

1. Introduction

Dating planetary terrains or surface modification by analyzing the size–frequency distribution (SFD) of impact craters has long been a fundamental technique (Shoemaker et al., 1962). The returned samples from the Apollo and Luna missions have established the absolute lunar surface ages at certain locations. These ages are then compared with the crater size–frequency distribution (CSFD) and density of the sampled sites to derive a crater production rate. Considering a constant impact flux on the Moon, model ages for the other parts of the Moon can be derived from the crater densities on the sampled surfaces. Since the 1960s, the crater counting methods have been greatly improved and different crater production functions have been established for the Moon, e.g., Hartmann (1970) and Neukum et al. (2001). The crater production functions then have been applied to Mars using the lunar impact history (Hartmann and Neukum, 2001; Ivanov, 2001; Neukum et al., 2001). Recently, they have even been extended to the outer Solar System satellites (Neukum et al., 2006; Schmedemann et al., 2012). All crater counting ages on other celestial bodies are based on certain assumptions about the origin and impact rate of the impactors.

On the Moon, small craters (diameter $D < 1$ km) are abundant and they are widely used to date relatively small surface areas (Hiesinger et al., 2012). However, the reliability of small crater counts has been questioned since the 1960s when the first lunar high resolution images were obtained (Shoemaker, 1965). It is well known that during impact processes, ejecta can travel long distances to produce secondary craters. Secondaries often occur in chains or clusters. However, many secondaries occur as isolated craters. These are distant secondaries which are circular in shape. Therefore, it is difficult to distinguish them from similar-sized primary craters. The unknown contribution of undetected secondaries can invalidate age dating (McEwen et al., 2005).

Many researchers were confident that the small crater populations could be used to date planetary surfaces (Werner et al., 2003; Michael and Neukum, 2010). However, this premise has been challenged recently. Chapman (2004), Bierhaus et al. (2005), McEwen et al. (2005) and McEwen and Bierhaus (2006) noted that the small crater populations on the Moon, Mars, and Europa were probably dominated by secondaries thus rendering age dating problematical. In response, Hartmann (2005, 2007), Ivanov (2006), Hartmann

* Corresponding author at: Lunar and Planetary Laboratory, University of Arizona, Tucson, AZ 85721, USA.
E-mail address: xiaobear@lpl.arizona.com (Z. Xiao).

0019-1035/$ - see front matter © 2012 Elsevier Inc. All rights reserved.
http://dx.doi.org/10.1016/j.icarus.2012.05.012

et al. (2008) and Werner et al. (2009) argued that small crater counts could be safely used with the Neukum and Hartmann production functions. They believed that the contamination by distant secondaries was minor and not a serious concern.

It has long been known that there is a steep upturn in crater size–frequency distribution curves at small diameters ($D < 1$ km). Whether it is caused by secondaries or primaries is a long controversy. Neukum and Ivanov (1994), Neukum et al. (2001) and Hartmann (2005) argued that this upturn was due to a change in the size–frequency distribution of primaries because the small primary projectiles have such steep size–frequency distributions. Ivanov (2006) claimed that most small craters ($D < 200$ m) at young lunar surfaces (age < 100 Ma) are primaries, while Hartmann (2007) believed that the ratio between small secondaries and primaries on lunar surfaces is an "open question". Neukum et al. (2001) believed that, except for distinct secondary crater clusters and chains, few distant secondaries exist on planetary surfaces and the majority of small craters are primaries. On the other hand, others maintain that the upturn in the SFD curves of small craters is the result of secondaries. Bierhaus et al. (2005) studied the distribution of secondaries on Europa, and found that 95% of Europa's small crater population is secondaries. When they applied the formation efficiency of Europa' secondaries to the Moon, they found secondaries could dominate the lunar small crater populations as well. McEwen and Bierhaus (2006) found that secondary craters should have a steeper size–frequency distribution than the collisional fragments. Bottke et al. (2005) and Bottke and Morbidelli (2006) found that the size–frequency distribution of small primary projectiles cannot account for the steep secondary branches in *R* plot curves. Strom et al. (2008) showed that on the martian young plains, the typical secondaries upturn occurs at about 1 km diameter while on Mercury the same upturn occurs at ~10 km.

Despite these controversies and new findings, researchers continue to disregard the potential problems of secondaries and continue to use the small crater populations to date planetary surfaces (e.g., Hiesinger et al., 2010; Zanetti et al., 2012). This paper tests the reliability of relative and absolute age dating using the small crater populations and looks into the reason for the problems.

2. Research materials and method

Four lunar surfaces with different stratigraphic ages were selected as the research areas (Table 1): Mare Nubium and the craters Alphonsus, Tycho, and Giordano Bruno. The small crater populations ($D < 1$ km) in these areas were studied using high resolution images from the Lunar Reconnaissance Orbiter Camera Narrow Angle Camera (LROC NAC, ~0.5–2 m/pixel; Robinson et al., 2005) and Kaguya Terrain Camera (TC, ~10 m/pixel; Kato et al., 2008).

The main procedure of this research is as follows:

First, we chose the counting areas from Kaguya and Lunar Orbiter images avoiding surface areas with obvious crater clusters or chains in an attempt to reduce the secondaries problem as others have done, e.g., Michael and Neukum (2010). Surfaces with bright impact rays that are composed of secondaries were eliminated. Also, to avoid the effect of mass wasting and other resurfacing events to the small crater populations, the counting areas are away from slopes and chaotic terrains. For each counting area, ~3–30 m is the confident diameter range for completeness and good-statistic of craters counted on LROC images, although larger and smaller craters were included; ~50–800 m is the confident diameter range for the Kaguya count.

Second, *R* plots and cumulative plots (Arvidson et al., 1979) were applied on the crater counts. We also calculated the absolute model ages (AMAs) for the counting areas after evaluating their saturation state. As others have done to derive model ages (Michael and Neukum, 2010), we used the "craterstats" tool (http://hrscview.fu-berlin.de/craterstats.html) and the Neukum production and chronology functions (Neukum et al., 2001).

Finally, the results are tested for consistency. For each counting area of its two size ranges, we compared the crater densities, the shape of the SFD curves in *R* plots, and the absolute model ages. For the results of two unsaturated counting areas (e.g., *A* and *B*), the following situations show that the small crater counts are problematic: in the *R* plots, *A* is older than *B* on the LROC images, but *A* is younger than *B* on the Kaguya images[1]; in the *R* plots, the two curves of *A* on the LROC and Kaguya images greatly vary from each other in the slope and density; in the cumulative plots, the two AMAs of *A* on the LROC and Kaguya images are significantly different; in the cumulative plots, the AMA of *A* is larger than that of *B* on the LROC images, but the AMA of *A* is smaller than that of *B* on the Kaguya images.

Table 1
Research areas in this paper.

Counting areas	Surface age	Coordinates
Mare Nubium	~3.85–2.77 Ga (Hiesinger et al., 2003; Bugiolacchi et al., 2006)	350°–0°E; −11° to −16°N
Alphonsus	>3.85 Ga (Zisk et al., 1991)	355.0°–359.4°E; −11.4° to −15.4°N
Tycho	~109 Ma (Stoffer and Ryder, 2001)	345°–352°E; −40° to −45°N
Giordano Bruno	~1–10 Ma (Morota et al., 2009)	101.5°–104°E; −35° to −36.5°N

3. Results

3.1. Mare Nubium and the Alphonsus crater

3.1.1. Counting areas

Alphonsus is a pre-Imbrium (>3.85 Ga) impact crater. It is located on the northeast border of Mare Nubium (Fig. 1). The crater floor consists of groups of rilles, fractures, a NNW-trending central ridge, and eleven dark halo craters (DHCs). Head and Wilson (1979) suggested that the DHCs were formed by intrusive volcanic activities which may have the same magma source as the adjacent Nubium lavas.

Since its formation, Alphonsus has been affected by many geological events, such as debris infilling from other impacts (Zisk et al., 1991) and the flooding of Mare Nubium (Head and Wilson, 1979). The evolution of Alphonsus can be determined from the cross-cutting relations of the various terrains in the crater floor (Fig. 1B). Considering the presumed relationship between the emplacement of Mare Nubium and the evolution of Alphonsus (Head and Wilson, 1979), three well studied Mare Nubium surfaces (Hiesinger et al., 2003; Bugiolacchi et al., 2006) and several geological units in the floor of Alphonsus were chosen as the counting areas (Fig. 2). The general information of the counting areas is listed in Appendix Table A.1.

3.1.2. R plot results

The DHCs 1–5 on the east crater floor and DHCs 9–11 on the west crater floor are covered by LROC images. Fig. 3 is the *R* plots of the counting areas at the dark haloed craters. It shows that the

[1] The vertical position of *R* plot curve (*R* value) is a measure of crater density or relative age on the same planet; the higher the vertical position, the higher the crater density and the older the surface (Strom et al., 2005, 2008.)

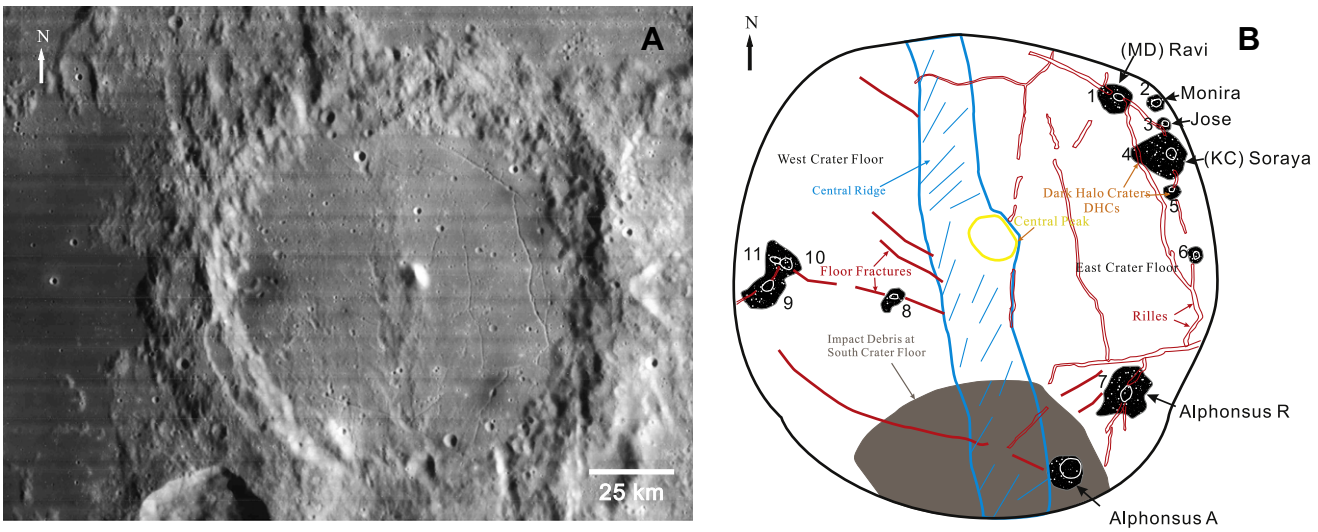

Fig. 1. (A) Alphonsus and Mare Nubium. The base image is from Lunar Orbiter IV (LO_4108_h2). Several low albedo dark patches at the crater floor named Dark Halo Craters (DHCs) have volcanic origin. (B) Schematic diagram of the different units at the crater floor. The eleven DHCs are numbered after Head and Wilson (1979). The white circles are the rims of the DHCs while the black areas are the dark deposits; white spots on the dark mantle materials represent small impact craters on the deposits. A group of fractures extending to the WNW occur at the west crater floor and cut through the central ridge, the west DHCs, and the south crater floor impact debris. At the south end of the central ridge is a debris deposit formed by the Arzachel impact to the south of Alphonsus (Coombs et al., 1990).

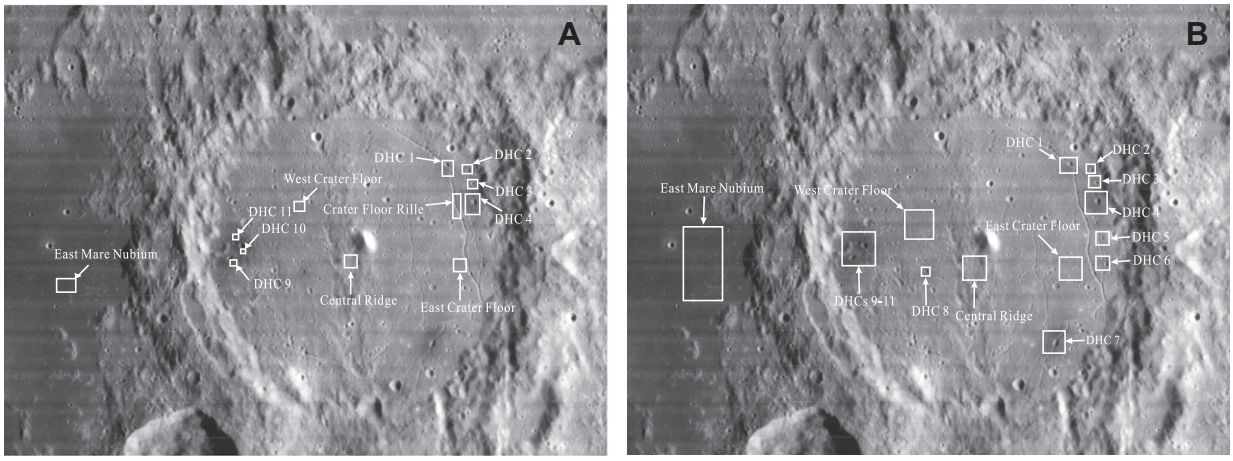

Fig. 2. Counting areas at the Alphonsus crater and Mare Nubium. (A) Counting areas on LROC images; (B) Counting areas on Kaguya images. The base image of both (A) and (B) is Lunar Orbiter 4108_h2. The squares are the counting areas and they are not to real scale. The "Mare Nubium Bright Area" and the "SE Mare Nubium Old surface" are two counting areas near the Lassell crater. Due to the vast surface area of Mare Nubium, the two counting areas are not shown in this figure. The detailed information of the counting areas is shown in Appendix Table 1.

DHCs 1–5 have similar size–frequency distributions and also little spread in the crater densities (Fig. 3A). The same is true for the DHCs 9–11 (Fig. 3B). However, when the curves of each group are combined, a distinct difference in the crater densities occurs between the DHCs 1–5 and DHCs 9–11 as the latter has a lower crater density (Fig. 3C). We will refer the DHCs 1–5 as "East DHCs" and the DHCs 9–11 as "West DHCs" respectively. Using lower resolution Kaguya images, one additional DHC on the west crater floor (DHC 8 in Fig. 2B) and two on the east crater floor (DHCs 6–7 in Fig. 2B) were included in the counts. DHCs 1–7 were combined as the "East DHCs" and DHCs 8–11 were combined as the "West DHCs" on Kaguya images (Appendix Table A.1).

Fig. 4 is a comparison of the crater counts on the LROC and Kaguya images for the crater floor (Fig. 4A), the Mare Nubium areas (Fig. 4B), the east and west DHCs (Fig. 4C), and the central ridge (Fig. 4D).

Fig. 4 shows the following results:

1. The crater densities of all the counting areas are smaller than 0.1 in R value.
2. The two R plot curves of a same counting area may significantly vary from each other in the slope (Table 2). For example, on the LROC side, the R plot curves for the east and west DHCs are relatively steep, with a differential slope about $p = -4$; however, on the Kaguya side, the curves are mostly flat with a differential slope of about $p = -3$ (Fig. 4C).
3. A gap occurs between the two curves of each counting area because craters in the 30–50 m diameter bins are not included. This is due to the relatively low resolution of Kaguya images and the relatively small counting areas on LROC images. The gap represents the crater density difference of the counting area at the large and small diameter ranges. For some counting areas, such as the east and west crater floor (Fig. 4A), their two R plot curves are consistent with a single curve because the gaps are small. However, for other counting areas, such as

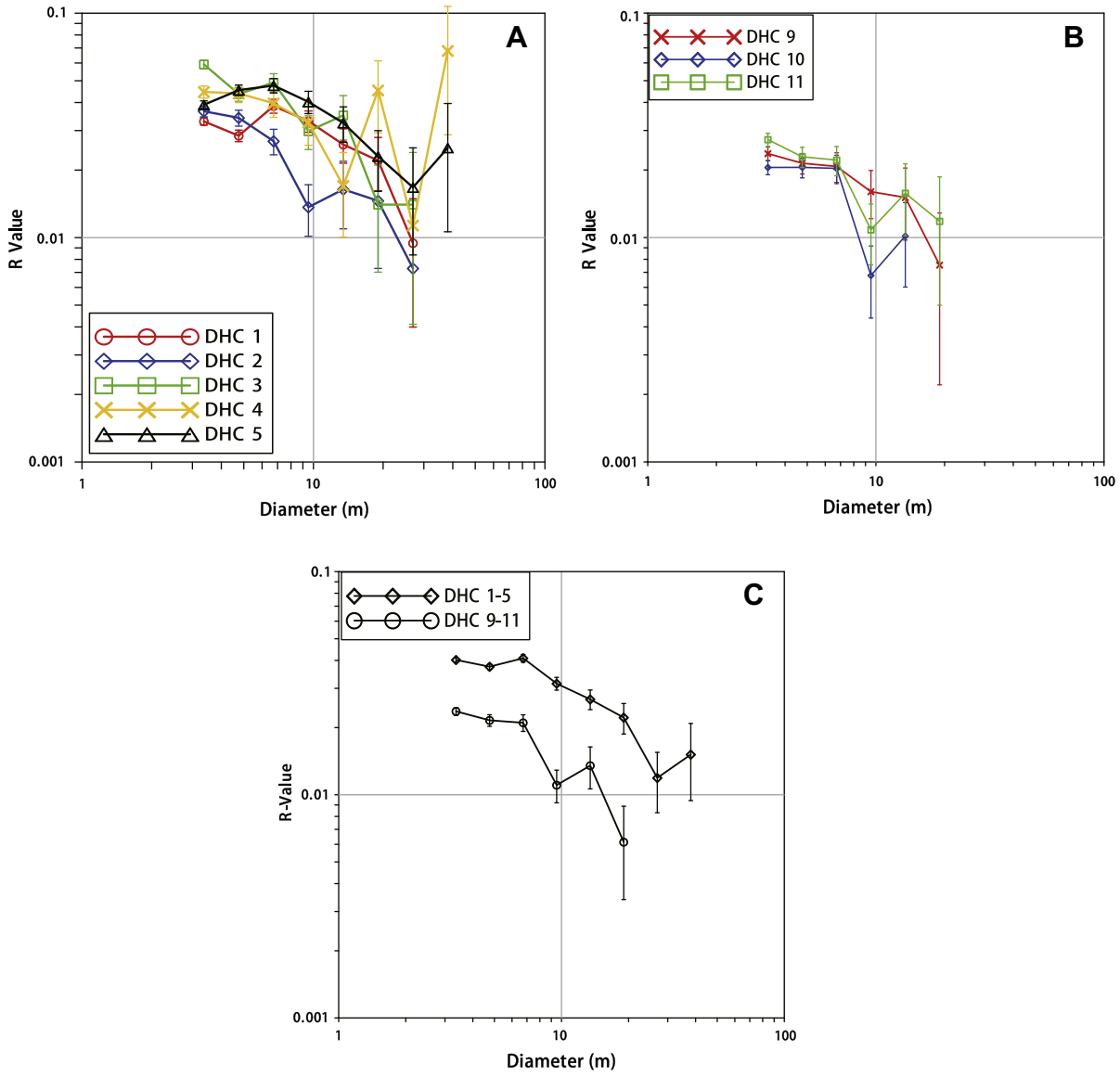

Fig. 3. *R* plot of the crater size–frequency distribution at the DHCs 1–5 (A) and DHCs 9–11 (B). All the crater counts are based on LROC images. The crater density of individual DHCs 1–5 is similar to each other as are those for the DHCs 9–11. (C) The DHCs 1–5 are grouped and compared with the DHCs 9–11. The former ones have a slightly larger crater density in average.

the east and west DHCs (Fig. 4C), their two curves are not consistent with a single slope because they greatly vary from each other in both the slope and *R* value (Table 2). It means that both the size–frequency distribution and crater density are different at the two diameter ranges of the same counting areas.

4. At the LROC side, the "West Crater Floor" appears to be older than the "East Crater Floor". However, at the Kaguya side, the two counting areas almost have the same crater densities and therefore the same relative ages (Fig. 4A).

3.1.3. Cumulative plot and absolute model ages

Judging by the crater saturation function of Hartmann (1984)[2], all the counting areas at Alphonsus and Mare Nubium are not saturated (Appendix Fig.A.1). Therefore, we calculated their AMAs using cumulative plots and the widely employed Neukum production and chronology functions (Neukum et al., 2001). The crater counting method follows that of Michael and Neukum (2010). The results are shown in Fig. 5. For any counting area, its two model ages on the LROC and Kaguya sides are significantly different from each other. In some cases, the difference can be as large as 100 times, e.g., the East Mare Nubium is dated to be ~ 26 Ma at the LROC side, but the model age is ~2.6 Ga at the Kaguya side. It is also shown by comparing the normalized crater density at 1 km, i.e., the $N(1)$ values in Fig. 5. No matter what are the real ages for the counting areas, the significant discrepancies between their model ages mean the small crater counts are problematic. More discussion about this discrepancy is in Section 4.

3.2. Tycho

3.2.1. Counting areas

Tycho is a rayed crater on the southern highlands of the lunar nearside. It is ~85 km in diameter (Fig. 6). Returned samples which are possibly from Tycho have an isotopic age of ~109 Ma (Stoffer and Ryder, 2001). In LROC and Kaguya images, craters on the floor of Tycho are difficult to discern because of the numerous fractures

[2] The saturation function of Hartmann (1984) is $N(D) = 0.047 * D^{-1.8}$ in cumulative plot. In *R* plot, it lies between the $a = 0.015$ and $a = 0.15$ saturation lines of Melosh (1989) and Gault (1970), $N(D) = a * D^{-2}$ and D is crater diameter.

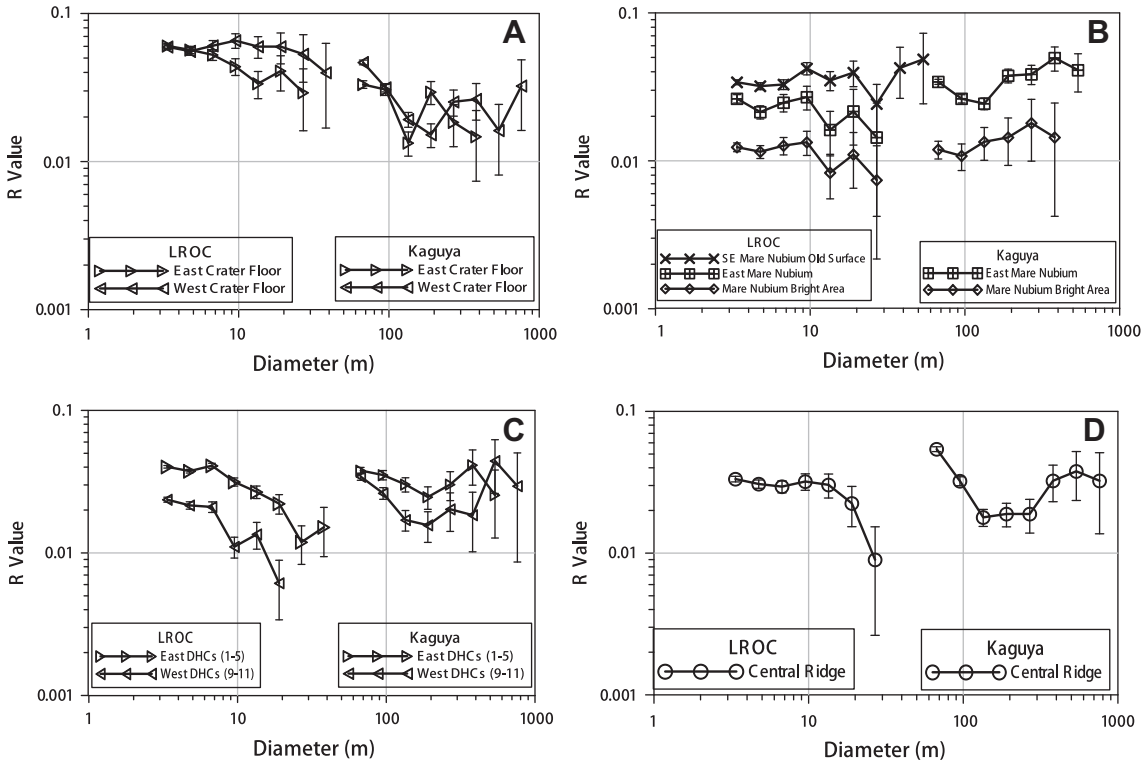

Fig. 4. *R* plot of the counting areas at the Alphonsus crater and Mare Nubium. The two curves of each counting area from the LROC and Kaguya counts are shown together. The shapes of the two curves of a same counting area always greatly vary from each other. The discrepancies in the results are discussed in Section 3.1.

and low relief mountains in the crater floor. Impact melt pools (IMPs) widely occur around the crater rim and they are mainly located on the east side (Fig. 6A). Fresh flow patterns occur on the crater wall and IMPs also form on the crater terraces (Fig. 6B).

Numerous studies have been focused on Tycho using small crater counts (Shoemaker et al., 1969; Dundas and McEwen, 2007). Recently, Hiesinger et al. (2010) and Hiesinger et al. (2012) dated model ages for several ejecta blanket areas and IMPs using small crater counts on LROC images. They found discrepancies in the AMAs of the same-aged terrains and they attributed it to the effect of different target properties. Plescia and Robinson (2011) confirmed the discovery of Shoemaker et al. (1969) that the density of small craters on the ejecta blanket of Tycho varies from place to place. They suggested that most of the small craters are the self-secondaries of Tycho.

During impact processes, impact melt and ejecta blankets form contemporaneously at geological time scale (Melosh, 1989). Therefore, dating the impact melt pools and ejecta blanket of Tycho should result in similar AMAs and the values should be ~109 Ma if this is the sample age of Tycho (Stoffer and Ryder, 2001). In this study, we chose several IMPs and ejecta blanket areas for the crater counts. The location of the counting areas is shown in Fig. 6. With LROC images, the counts were made on an IMP on the north crater rim, an IMP on the east crater terrace, two IMPs on the NE crater rim (Fig. 6C), an IMP at the foot of the central peak (Fig. 6D), and an ejecta blanket area (Fig. 6A). With Kaguya images, all the IMPs on the east crater rim were combined because most of them coalesce with each other forming a common unit. The general information of the counting areas is listed in Appendix Table A.2.

3.2.2. R plot results

Fig. 7 shows the *R* plots of the crater counts at Tycho. Due to the limited counting areas on LROC images (Appendix Table A.2), the number of the counted craters larger than 10 m diameter was not adequate for good-statistic in *R* plots. The size–frequency distributions show that:

1. The four IMPs have almost the same crater densities on LROC images.
2. At both the LROC and Kaguya sides, the ejecta blanket has larger crater density than the IMPs.
3. Unlike the complicated SFD curves of the counting areas at Alphonsus and Mare Nubium (Fig. 4), those at Tycho have relatively simple and uniform shapes. The counting areas have steep slopes at both the LROC and Kaguya sides (Table 3), which are identical to the SFD curves of typical secondaries on Mars (Strom et al., 2008).

Table 2
The differential slope of the *R* plot curves for the counting areas at the Alphonsus crater and Mare Nubium.

Counting areas	LROC[a]	Kaguya[a]
Central Ridge	−3.467	−3.035
Crater Floor		
East Crater Floor	−3.338	−3.395
West Crater Floor	−3.109	−3.286
DHCs		
East DHCs	−3.500	−2.905
West DHCs	−3.725	−2.695
Mare Nubium		
SE Mare Nubium Old Area	−2.995	–
East Mare Nubium	−3.228	−2.957
Mare Nubium Bright Area	−3.211	−2.791

[a] On a *R* plot, a $p = -3$ distribution plots as a horizontal straight line; a $p = -2$ distribution slopes down to the left with an angle of 45°, and $p = -4$ distribution slopes down to the right at 45° (Strom et al., 2005).

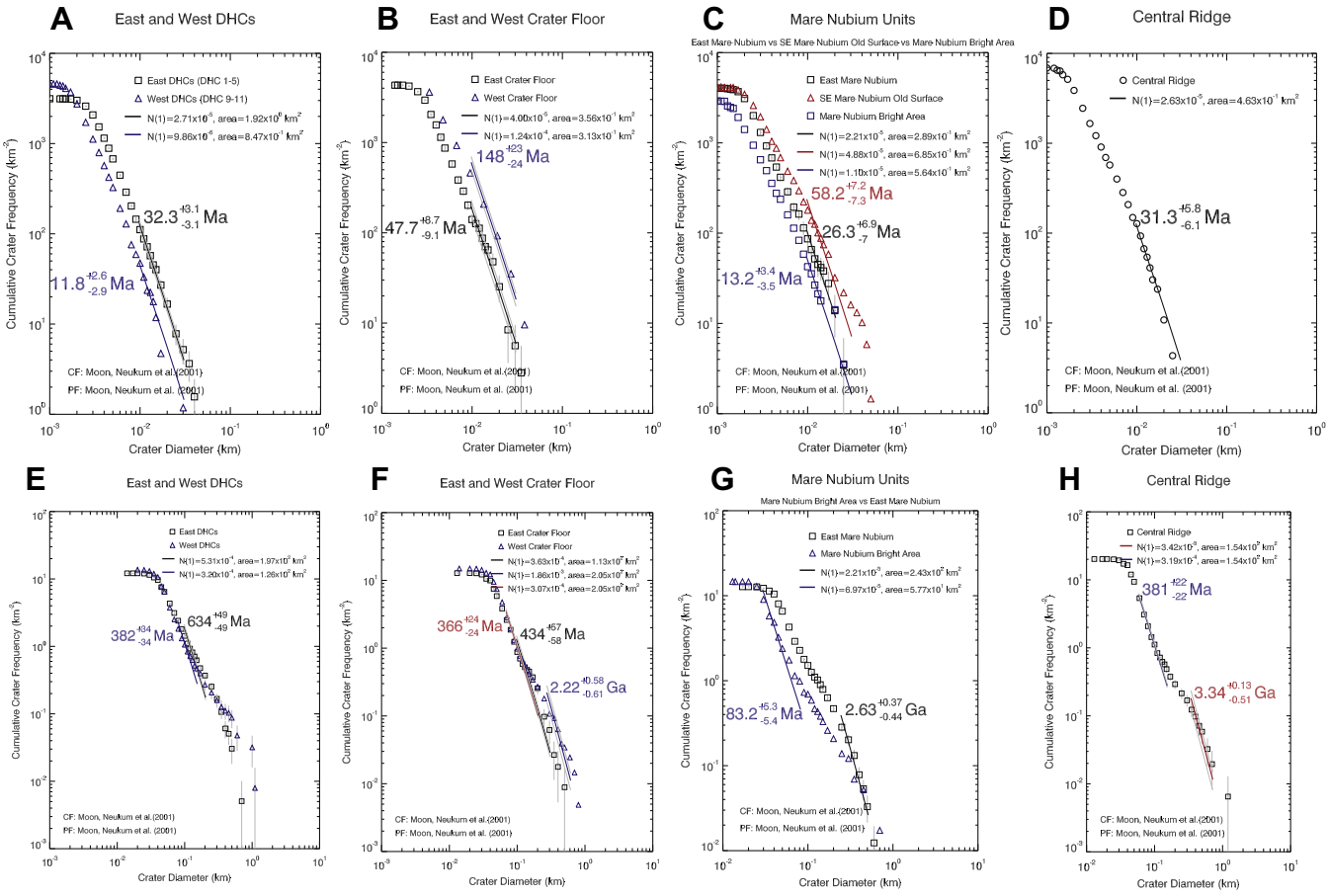

Fig. 5. The absolute model ages of the counting areas at the Alphonsus crater and Mare Nubium. The upper row lists the model ages derived from the crater counts on LROC images, the lower row lists those on Kaguya images. PF means production function and CF means chronology function. The diameter fitting ranges are larger than 10 m in all the counts and the errors are calculated following the method in Michael and Neukum (2010). Referring to the advocated method in Michael and Neukum (2010), the 366 Ma age in (F) should represent a resurfacing age for the "West Crater Floor", the same is true for the 381 Ma age for the central ridge in (H). Great discrepancies occur in the two model ages for any counting area. See Section 3.1.3 for discussion.

However, discrepancies also occur in the crater counts. The two curves of the ejecta blanket have a small gap between them indicating a consistent crater density. On the contrary, the gap between the curves of the IMPs is so large that they cannot be considered as one curve (Fig. 7). It means the crater density of the IMPs at the larger diameter range (Kaguya side) is significantly greater than that at the smaller diameter range (LROC side). The nonuniformly distributed secondaries in different diameter ranges are a possible reason for this discrepancy and it is discussed in Section 4.1.

3.2.3. Cumulative plot and absolute model ages

The counting areas at Tycho are not saturated when evaluated by the equilibrium function of Hartmann (1984) (Appendix Fig.A.1). Since the Neukum production function claims to be valid for craters from 10 m to 300 km in diameter (Neukum et al., 2001), the AMAs for the counting areas at Tycho are calculated by best fitting lines at diameter larger than 10 m. Fig. 8 shows the result.

Both the Kaguya and LROC AMAs show that the ejecta blanket is older than the IMPs, which is consistent with the *R* plot results (Fig. 7). However, the counting areas should have a same model age at both the LROC and Kaguya sides. On the contrary, the two AMAs of the ejecta blanket are different by a factor of ~3, and those of the IMPs are different by a maximum factor of ~30. Moreover, none of the AMAs are even close to 109 Ma. The same problems were noticed by Hiesinger et al. (2010) and Hiesinger et al. (2012). Their AMAs for the IMPs were ~35 Ma while those for the ejecta blanket were ~100 Ma (Hiesinger et al., 2010). van der Bogert et al. (2010) and Hiesinger et al. (2010) ascribed this discrepancy to the different properties of target materials, i.e., the IMPs has stronger strength than the porous ejecta blanket therefore a same-sized projectile may form different sized craters on these two surfaces. While this factor may cause the observed different crater density, the effect of target properties to model ages was not numerically evaluated. Moreover, we counted craters on the IMPs as Hiesinger et al. (2010) did using the same data set in a same diameter range. Our AMAs are ~10 times smaller than those of Hiesinger et al. (2010). Therefore, besides different target properties, other factors may also affect the density of small craters at same aged terrains. In Section 4.1, we suggest that the small crater populations are dominated by secondaries and their nonuniform distribution may contribute to the different crater densities at different locations.

3.3. Giordano Bruno

3.3.1. Counting areas

Giordano Bruno is the freshest complex crater on the Moon. It is ~22 km in diameter and the crater floor is full of impact melt and disturbed impact debris (Fig. 9). Since Hartung (1976) first claimed that this crater was formed ~800 years ago quoting ancient monks' description of an impact event on the Moon, different arguments about its age have been proposed. Recently, Morota et al. (2009)

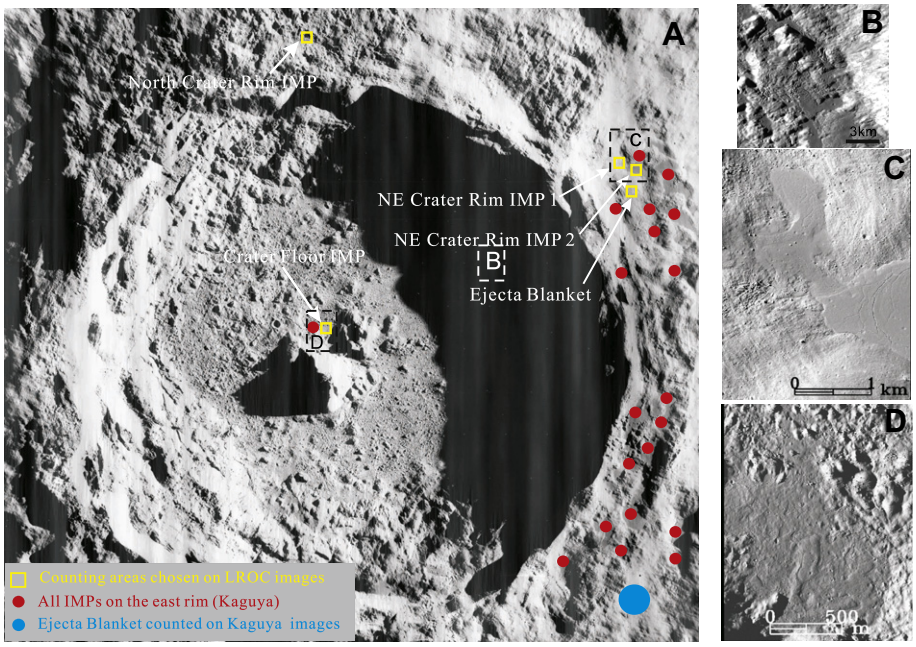

Fig. 6. Tycho crater shows the counting areas on the base image LO 5125_med. (A) The counting areas based on LROC images are shown as yellow squares. Because the east crater wall is covered by shadow, the "Crater Terrace IMP" is not shown in (A) and it is in (B). The counting areas based on Kaguya images are indicated as red dots for the impact melt pools (IMPs) and blue dot for the ejecta blanket. None of the counting areas are to scale. (B) Flow traces occur on the NE crater wall. When the impact melt flowed down the crater rim, they cooled during the drainage. The melt then accumulated on the crater terraces forming IMPs. The base image is TC_EVE_02_S42E348S45E351SC. (C) The "NE Crater Rim IMP 1" (right) and "NE Crater Rim LMP 2" (left). The boundary between the two IMPs is near the center of the image. The base image is LROC M119916367R. (D) The IMP at the foot of the central peaks shows the albedo difference between the IMP and the crater floor. The base image is LROC M102230053L.

counted 49 craters larger than 40 m diameter at a 294 km^2 area on the ejecta blanket of Giordano Bruno using Kaguya images (Fig. 9). They derived a model age of ~1–10 Ma for the crater and suggested that ~4 Ma was the confident model age. Plescia et al. (2010) found that small craters on the ejecta blanket of Giordano Bruno are not uniformly distributed, just like those on the ejecta blanket of Tycho. They suggested that the small craters were self-secondaries of Giordano Bruno and this crater could be as young as 800 years.

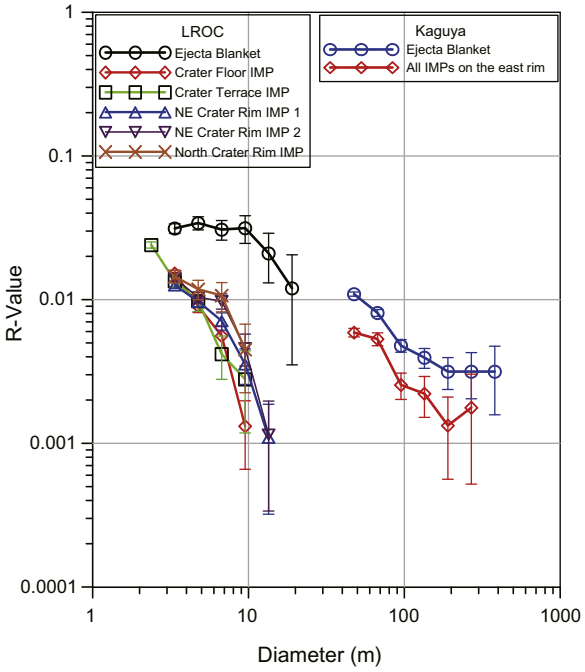

Fig. 7. *R* plots of the crater counts at the Tycho crater. The left curves are from LROC counts while the right ones are from Kaguya counts. The two groups of curves for the impact melt pools have different crater densities. A probable reason is that most of the small craters are secondaries. See the detailed discussion in Section 4.1.

To test the reliability of small crater counts, we counted craters on the same area as that of Morota et al. (2009) using Kaguya images (Fig. 9). Furthermore, large surfaces at the west crater rim are covered by scattered boulders and some are larger than 30 m in diameter. These areas may be deficient in craters due to the lighting conditions and the large boulders prohibit small impact craters from forming. Therefore, these areas were excluded from our Kaguya counting area (Fig. 9). To confirm the potential crater density difference on the continuous ejecta blanket (Plescia et al., 2010), ten same-sized rectangular areas were selected on the continuous ejecta blanket using LROC images. Four are located on the northern blanket and six on the southern blanket (Fig. 9). They have different distances from the crater rim. Due to the large size of the rectangular areas (~9.6 km^2), craters larger than 7 m in diameter were counted on these areas. They were then combined to compare with the crater count on Kaguya images. Because most of the craters on the continuous ejecta blanket are small (D < 10 m), in case the crater density differences are not show for

Table 3
The differential slope of the *R* plot curves for the counting areas at the Tycho crater.

Counting area	LROC	Kaguya
Ejecta blanket	−3.962[a]	−3.621
Crater floor IMP	−5.255	−3.850
Crater terrace IMP	−4.158	
NE crater rim IMP 1	−4.700	
NE crater rim IMP 2	−4.680	
North crater rim IMP	−4.041	

[a] This value is for the steep segment of the curve at the 10–30 m diameter range.

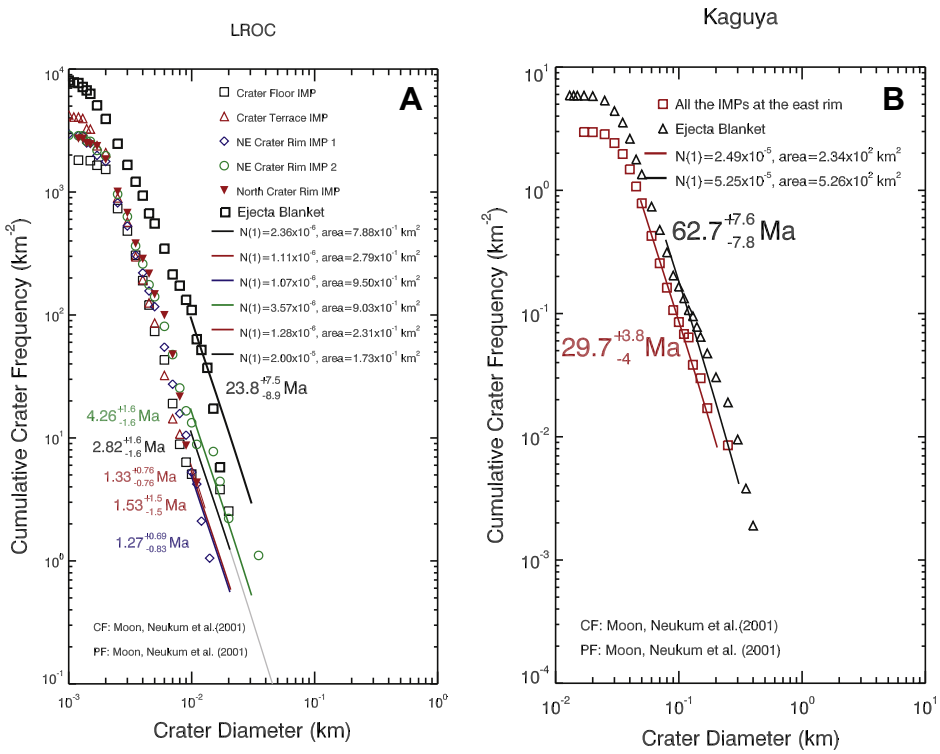

Fig. 8. Absolute model ages for the counting areas at Tycho. CF is crater chronology function and PF is crater production function. The model ages are calculated following the method in Michael and Neukum (2010). (A) The model ages from the LROC counts. The diameter fitting ranges are larger than 0.01 km. (B) The model ages derived from the Kaguya counts with the diameter fitting ranges larger than 0.05 km. Great discrepancies occur in the two model ages of any counting area and none of the ages is close to the real age of Tycho. Probable reasons for this discrepancy is discussed in Section 4.1.

craters larger than 7 m in the ten rectangular areas, seven straight lines on the southern continuous ejecta blanket were selected. The lines are away from the hummocky crater rim and the local slope is small than 4°. The lines have equal lengths and increasing distances from the crater rim (Fig. 9). Caters larger than 2 m diameter which transect the lines were counted and compared. The general information of the crater counts is given in Appendix Table A.3.

3.3.2. R plot results

We compared the crater densities on the ten rectangular counting areas. On the northern ejecta blanket, the left areas L-N1 and L-N2 and the right areas R-N1 and R-N2 were compared. The same was done for the left and right areas on the southern ejecta blanket. Fig. 10 is the result. It shows that no significant crater density differences occur on the continuous ejecta blanket in the 7–30 m diameter range. We then compared the number of craters which transect the seven dashed lines (Fig. 9). The result in Fig. 11 shows that the crater density increases with the distance from the crater rim, which is consistent with the finding of Plescia et al. (2010) that the crater density is different across the ejecta blanket. This result further shows that the density difference is mainly for craters smaller than 7 m diameter.

Fig. 10 shows that the crater size–frequency distribution curves at the ten rectangular areas have uniformly steep slopes which are similar to that of typical secondaries. Combining the ten rectangular areas and comparing it with the ejecta blanket counted on Kaguya images, the *R* plot result shows that the two curves are almost the same in both the shape and slope (Fig. 12). Unlike the *R* plot curves in Figs. 4 and 7, the gap between the two curves of the ejecta blanket is relatively small as the two error bars at $D = \sim 30$ m almost cross each other (Fig. 12). Therefore, the two curves can be taken as the two parts of a continuous curve. In general, except for the nonuniform distribution of the small carters, no obvious discrepancy occurs in the *R* plot results.

3.3.3. Cumulative plot and absolute model ages

The craters on the ejecta blanket are not saturated because the crater densities are too low (Fig. 12). Cumulative plots are then performed to calculate the AMAs (Fig. 13). Similar to the result of Morota et al. (2009), both of the two AMAs are between 1 and 10 Ma with a difference of a factor of ~2. Therefore, no obvious discrepancy occurs for the two AMAs. However, these ages are possibly based on secondaries making them problematic (see the detailed discussion in Section 4.1).

4. Discussion

4.1. The population of secondaries

To settle the disagreement about the origin of steep upturns in CSFD curves (Hartmann, 2005; Bierhaus et al., 2005), we need to distinguish the size–frequency distributions of small secondaries and primaries. Since secondaries originate from impacting of ejected boulders, the size–frequency distribution of impact ejected boulders is a direct measurement for the projectiles of the secondary populations. Bart and Melosh (2007) counted boulders around small and fresh lunar impact craters and believed that the size–frequency distribution of the boulders is the same for those ejected from larger impact craters. In comparison, the SFD of the impact ejected boulders has the same steep slope as that of the small crater populations at Tycho and Giordano Bruno (Fig. 14). This relationship supports that secondary populations have a steep size–frequency distribution curve. On the other hand, McEwen et al. (2005) counted secondaries around the martian Zunil crater, and their crater count data shows that the martian secondaries have a similar steep upturned slope (Fig. 14). This is consistent with the slope of the interpreted secondaries population on the martian young plains (Fig. 14; Strom et al., 2008). These observations are

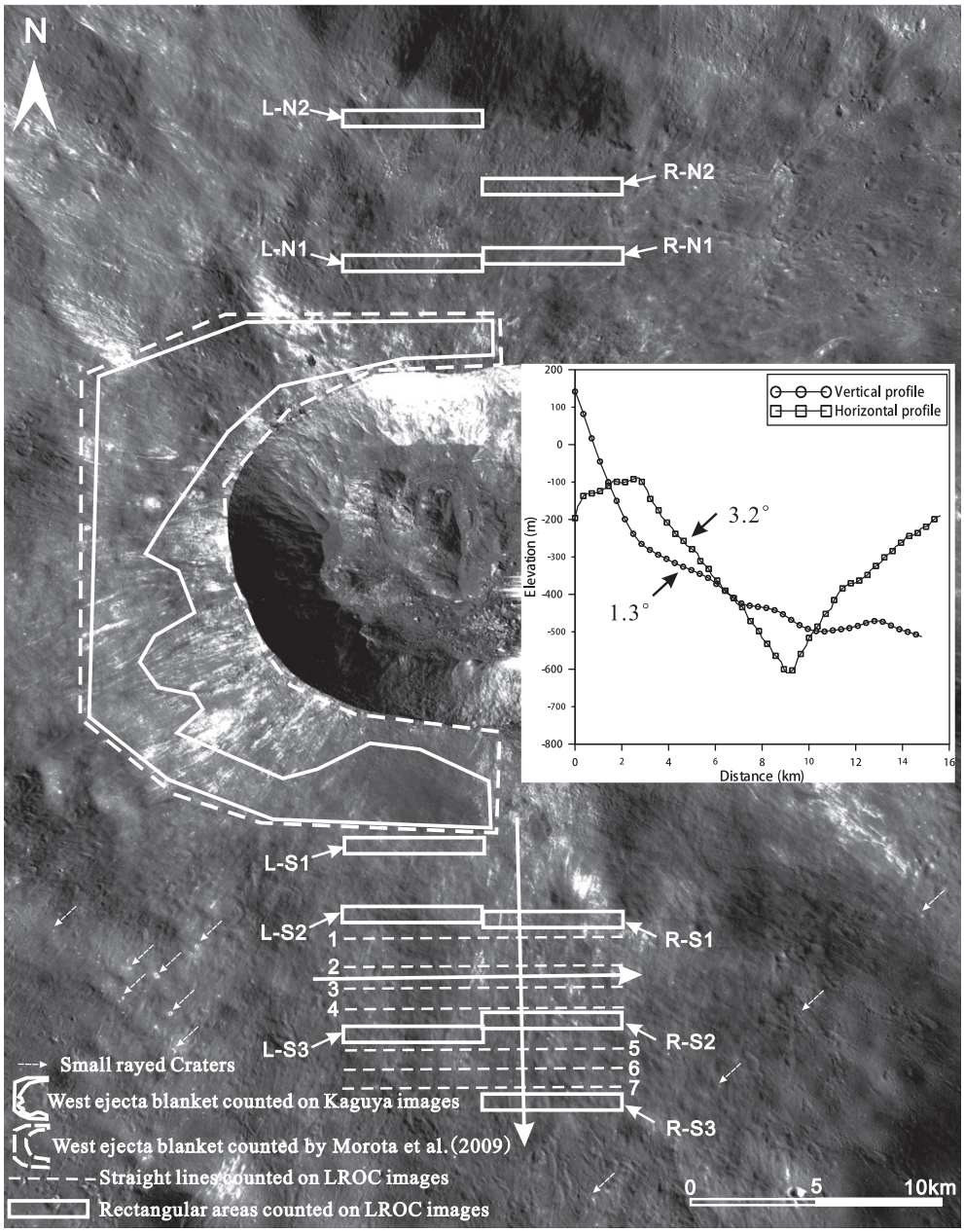

Fig. 9. Giordano Bruno showing the counting areas, which include: the west ejecta blanket counted by Morota et al. (2009) is the white dashed area; the west ejecta blanket counted on Kaguya images in this paper is the white solid area; the ten equal-sized rectangular areas on the continuous ejecta blanket have an increased distance from the crater rim for those at the same side; the seven straight lines on the southern ejecta blanket have equal-length and increasing distance from the crater rim. Examples of small rayed craters with probable primary origin are indicated as white arrows. The rayed craters are randomly distributed on the continuous ejecta blanket. The vertical and horizontal arrowed lines on the south ejecta blanket are LOLA topography profiles with a resolution of 512 pixel/degree. The inset figure shows the two topography profiles. The unit of the *x*-axis is in kilometer and the *y*-axis is in meter. The base images are Kaguya TC: TCO_MAP_02N39E102N36E105SC and TCO_MAP_02N36E102N36E105SC.

consistent with the argument that the secondaries populations on the Moon and Mars have steep upturns.

The *R* plot curves of the counting areas at Tycho have steep upturned slope (Fig. 7) indicating the small crater populations may be dominated by secondaries. Two observations further support this interpretation: (1) The crater density on the continuous ejecta blanket is different from that on the IMPs, which is inconsistent with the fact that the two units were formed at the same time as the Tycho impact. Different target properties may affect the sizes of craters for a given-sized projectile and this could be a reason for the observed crater density difference (van der Bogert et al., 2010). However, IMPs have different model ages in different crater counts, i.e., the model ages of IMPs in our LROC counts (Fig. 8) and those form Hiesinger et al. (2010) are different by a maximum factor of ~30. A possible reason is that the small crater populations at these surfaces are dominated by nonuniformly distributed secondaries (Shoemaker et al., 1969). This will cause different crater densities at different locations, even for same-aged terrains with same target properties. (2) The gap between the two *R* plot curves of the ejecta blanket is caused by a crater density difference between the large and small diameter ranges. No obvious resurfacing events which may cause different crater densities are seen on the counting areas. Assuming the ejecta blanket has nonuniform properties at different depths (strength, porosity, etc.), this may cause the observed crater density different of the ejecta blanket at the different diameter ranges. Another possible reason is that secondaries dom-

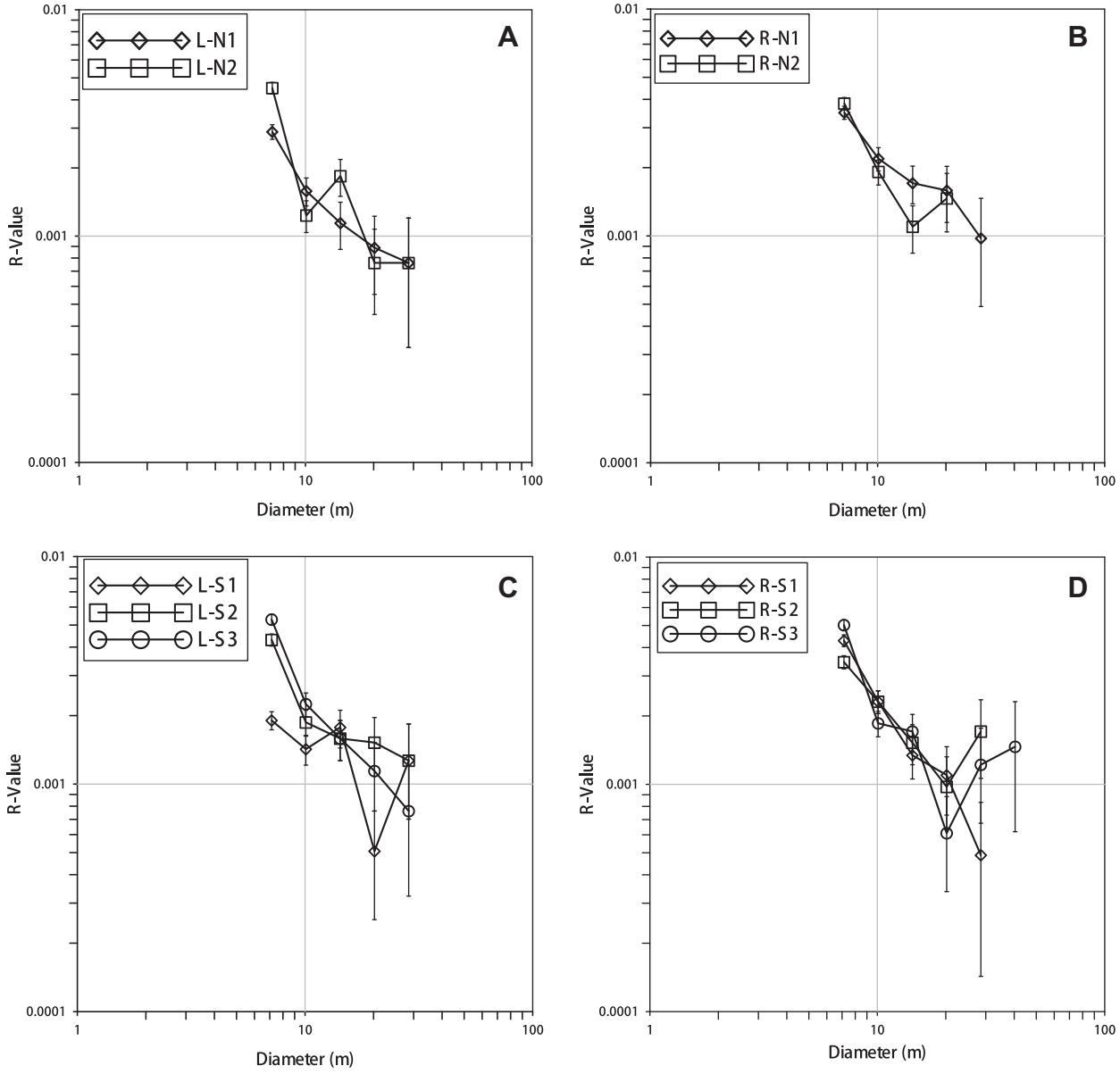

Fig. 10. Crater size–frequency distributions for the ten rectangular counting areas on the continuous ejecta blanket of Giordano Bruno are presented in *R* plot. No significant crater densities differences are seen on the continuous ejecta blanket for craters larger than 7 m in diameters. All the curves have steep slopes.

inate the small crater populations at Tycho and the crater density varies with diameter ranges.

Moreover, the SFD curve of Tycho's ejecta blanket rolls over at diameter smaller than 10 m, which is different from the curves of the IMPs at the same diameter range (Fig. 7). Three possible reasons may explain this: (1) The SFD of secondaries must roll-over at some diameter value, i.e. the craters in a cluster cannot continue down at a steep power-law slope (i.e., $p = \sim -4$ in *R* plot) to arbitrarily small sizes. (2) Craters smaller than 10 m in diameter on the continuous ejecta blanket were partly removed by some post-impact processes. (3) Young surfaces, such as the Tycho crater, are the regions expected to be least affected by secondary craters. The presence of a shallow sloped crater SFD on the ejecta blanket at $D < 10$ m may be evidence for a potential shallow primary crater population at these sizes.

The counting areas at Giordano Bruno also have steep SFD curves (Figs. 10 and 12). Although this crater is extremely young and no obvious discrepancies occur in the crater counting results (Figs. 12 and 13), three observations suggest that most of the small craters are possibly the self-secondaries from Giordano Bruno: (1) Zanetti et al. (2012) reported a distinct trend of decreasing crater density ($D = 1.5$–150 m) with increasing distance from the crater rim of four large Copernican-aged impact craters (Aristarchus, Copernicus, Jackson, and Tycho). They suggested that most of the small craters were self-secondaries of their parent craters which caused the observed density difference. However, we found an opposite trend on the continuous ejecta blanket of Giordano Bruno, i.e., the density of the small craters ($D = 2$–7 m) increases outward from the crater rim (Fig. 11). While mass wasting and late impact melt flow may reduce the crater density on the continuous ejecta blanket towards a larger distance from the crater rim, the movement behavior, spatial distribution, and emplaced-time of high-trajectory ejecta in impact processes are important to solve this controversy. In the case of Giordano Bruno, mass wasting may not be effective enough to cause the observed crater density difference on the continuous ejecta blanket. The Lunar Orbiter Laser Altimeter (LOLA) profiles crossing

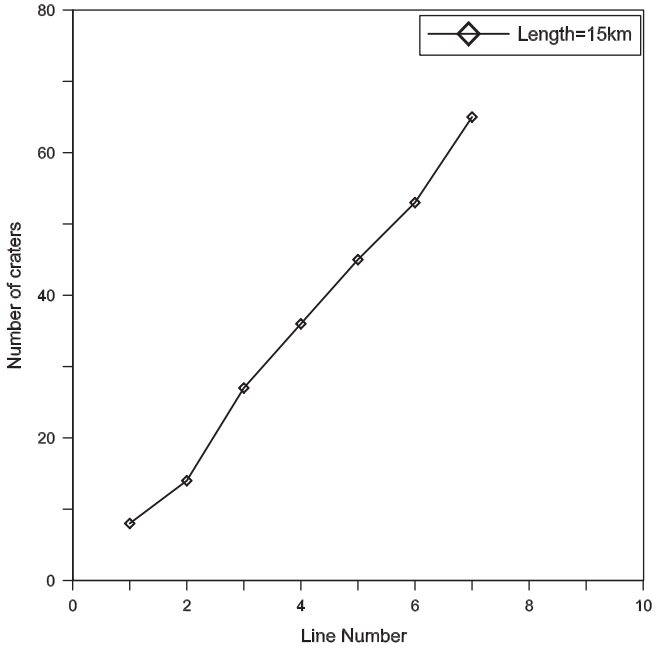

Fig. 11. Comparison of the number of craters which transect the seven dashed straight lines in Fig. 9. Craters larger than 2 m diameter are included. All the dashed lines are 15 km long and are of increasing distance from the crater rim. The number of craters increases with the distance from the crater rim (see Section 4.1 for detailed discussion).

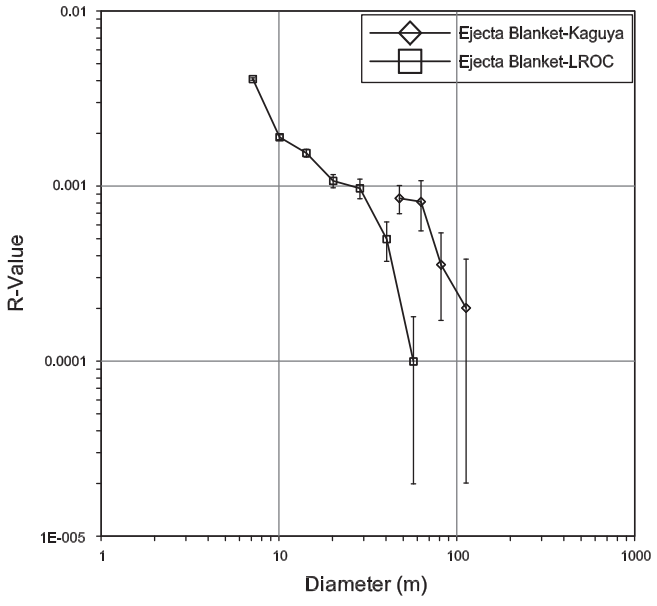

Fig. 12. Comparison of the crater size–frequency distributions on the continuous ejecta blanket of Giordano Bruno based on the LROC and Kaguya counts. Both of the curves have steep slopes which are typical for secondaries.

the nine lines in Fig. 9 show that the local slope is less than 4° (the vertical axis is in meter and the horizontal axis is in kilometer in the inset). It is more likely that the crater density difference is caused by the nonuniformly distributed secondaries across the ejecta blanket. (2) Most of the small craters do not have pristine morphologies (i.e., sharp raised rim), probably because the ejecta blanket was still unconsolidated when the ejecta impacted on it with a relatively low velocity (Plescia et al., 2010). (3) Rays of small craters may be thin layers of ejecta distributed by the impacts (Shoemaker, 1962), or they can be caused by compositional contrast with surrounding terrains (Hawke et al., 2004). Most, but not all, of the small craters on the continuous ejecta blanket of Giordano Bruno do not have rays. If the rays of small primaries (D = ~10 m) form as thin layers of impact deposit, considering the slow erosion rate on the Moon (Ashworth, 1978; Dundas and McEwen, 2007), the rays of the small primaries on the ejecta blanket of Giordano Bruno should be little eroded even assuming an age of 1–10 Ma. Therefore, most of the small craters on the continuous ejecta blanket of Giordano Bruno are possibly its self-secondaries. The AMAs derived from the small crater counts in Fig. 13 are possibly based on secondaries which invalidate the ages.

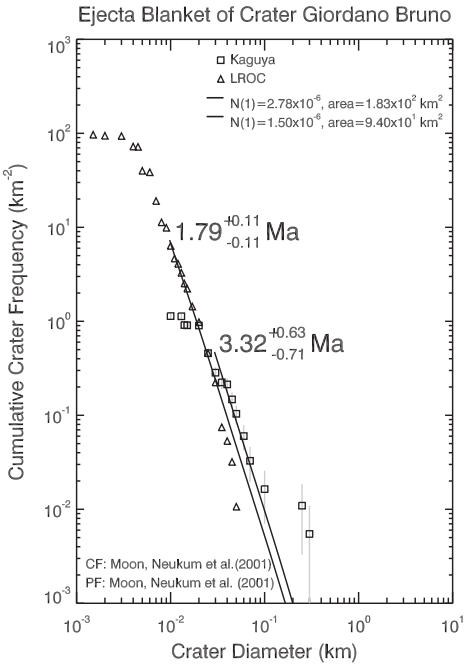

Fig. 13. Absolute model ages for the continuous ejecta blanket of Giordano Bruno. CF is crater chronology function and PF is crater production function. The diameter fitting range for the Kaguya counts is 0.03–1 km while that for the LROC counts is 0.01–1 km. The ejecta blanket at the LROC side is combined from the ten rectangular areas. The errors of the ages are calculated after the method of Michael and Neukum (2010). The model age derived by Morota et al. (2009) is 1–10 Ma and our results are within this range. However, the crater counts may be actually performed on the self-secondaries or Giordano Bruno which invalidate the ages. See section 4.1 for discussion.

The small crater populations at Alphonsus and Mare Nubium do not have steep size–frequency distribution slopes as that of typical secondaries (Fig. 4). Does it mean that the counted small craters at these surfaces are mostly primaries? A Tycho-size impact crater on the Moon can produce 10^6 secondaries larger than 63 m diameter (Dundas and McEwen, 2007) and the majority of them are distant secondaries. Bierhaus et al. (2005) suggested that small crater populations on the Moon (D < 1 km) could be dominated by secondaries. Considering the counting areas at Mare Nubium and Alphonsus are fairly old, the small crater populations (D < 1 km) on these surfaces may have well been dominated by secondaries. On the other hand, crater saturation may change SFD curves at certain impactor populations and the equilibrium densities always occur at ~R > 0.1 (Richardson, 2009). In this study, our counting areas do not reach this equilibrium density or that of Hartmann (1984). Therefore, crater saturation may not be suitable to explain the observed discrepancies in this case. Ancient resurfacing events, mass wasting, different impactor population, nonuniformly distributed distant secondaries, illumination condition (Wilcox et al., 2005; Ostrach et al., 2011), and different erosion rates for different sized craters are all possible reasons for the observed discrepancies in these crater counts. However, it may not be possible to uniquely distinguish

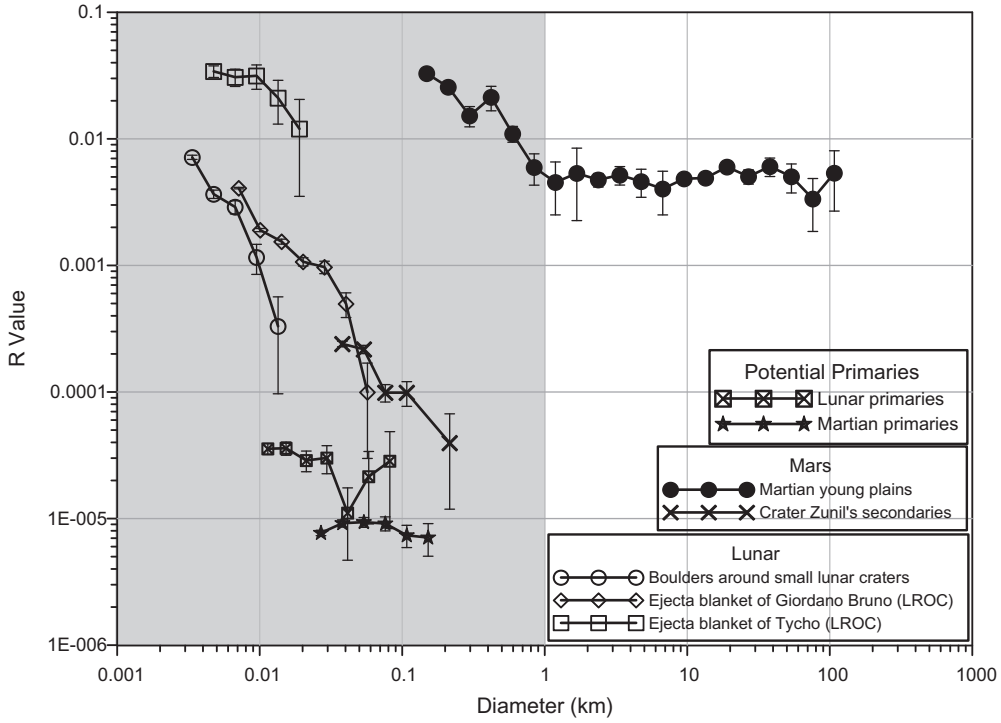

Fig. 14. *R* plots of the following crater counts: the impact ejected boulders around small fresh lunar craters (data from Bart and Melosh (2007)); small craters on the ejecta blanket of Tycho on LROC images (Fig. 7); small craters on the ejecta blanket of Giordano Bruno on LROC images (Fig. 12); the Population 2 craters at the martian Young Plains (Strom et al., 2008); martian crater Zunil's secondaries (data from McEwen et al. (2005)); the small rayed craters on the continuous ejecta blanket of Giordano Bruno which are probably lunar primaries; the small rayed craters on Mars which are probably martian primaries. The shaded band marks the small crater populations ($D < 1$ km). Except for the potential lunar and martian primaries, the other size–frequency distribution curves in this band have steep slopes. The probable small primaries populations have flat curves which appear to be part of the Population 2 craters in the size-frequency distribution. The plots support that the steep upturns at crater size–frequency distributions are caused by secondaries not primaries.

between these factors. In general, the reason for the detected discrepancies in the crater counts at Mare Nubium and Alphonsus needs more work to be resolved.

The contamination of secondaries invalidates the interpretation of crater counting results (McEwen and Bierhaus, 2006). The fundamental reason is that distant secondaries are made by high-velocity ejecta and are circular in shape making them difficult to be distinguished from primaries. Hartmann (2005) argued that the Hartmann production function was derived from large surface areas which already included the effect of distant secondaries. However, the local ratio of secondaries and primaries is uncertain (Hartmann, 2007). Using the averaged production function and localized crater densities to calculate absolute model ages have large uncertainties. To get a relatively reliable model age from small crater counts, besides an up-to-date knowledge of the present impact flux, we also need to know the size-frequency distribution of primaries.

4.2. The population of potential primaries

Although secondaries dominate the small crater populations on the Moon, a substantial number of primaries must exist in the small crater populations. On the Moon, the best place to look for small primaries ($D < 1$ km) is on young surfaces. Giordano Bruno has pristine and large areas of relatively smooth continuous ejecta blanket (Fig. 9). Most of the small craters on the continuous ejecta blanket are possibly secondaries as discussed in Section 4.1. Another population of small craters has sharp morphologies and fresh rays, e.g., several examples are indicated by the white arrows in Fig. 9. The crater erosion rate on lunar surfaces is ~2–6 cm/Myr (Dundas and McEwen, 2007) and the abrasion rate of kilogram-sized lunar rocks by micrometeoroid bombardment is ~1 cm per 10^7 yr (Ashworth, 1978). Superficial rays of primary craters ~10 m in diameter on the continuous ejecta blanket of Giordano Bruno should be little eroded even assuming an age of 1–10 Ma for the crater. The rayed craters are probably primaries postdate Giordano Bruno. Under this consideration, on a 1380 km^2 area of the continuous ejecta blanket, we collected ~220 rayed craters larger than 8 m in diameter. Two more observations support their primary origin: (1) The spatial density of secondaries on the continuous ejecta blanket is not uniform (Fig. 11), but the rayed craters are randomly distributed (Fig. 9). (2) The SFD curve of the rayed craters is different from that of typical secondaries. It has a flat slope which is identical to the Population 2 craters on the inner Solar System bodies (Strom et al., 2005; Fig. 14).

On Mars, the surface erosion rate is much higher than that on the Moon (Smith et al., 2008). Small craters and their impact rays are easily obliterated. Therefore, the presently observed small rayed craters on Mars ($D < 1$ km) are very young and they probably represent the newly formed martian primaries. About 900 small rayed craters larger than 20 m in diameter are collected on a 1.128×10^5 km^2 martian surface.[3] The *R* plot shows that both the potential lunar and martian primaries have relatively flat size–frequency distribution curves, which are distinctively different from those of small secondaries (Fig. 14). Furthermore, the two curves seem to be a continuation of the SFD curve of the Population 2 craters from larger diameters (Fig. 14). These data provide evidence

[3] The counts were performed by Robert G. Strom and Natasha Johnson (now at Goddard Space Flight Center) based on Viking Orbiter images.

that small primaries have a flat size–frequency distribution curve and the steep curves at the small diameter ranges may not be caused by primaries.

4.3. Uncertainties caused by crater counters

Decimeter-scale resolution images are becoming available for more and more celestial bodies. In the future, small crater counts may be vastly used for small-scale geological study. Without cautious and a full understanding of the potential problems in small crater counts, invalidate interpretations may ruin these studies. Nowadays, crater counts are mainly performed by bare eyes. The precision of small crater counts highly depends on a counter's experience and his/her criteria in identifying impact craters. Crater-count is a subjective process and different people may have different crater counting result for a same area with a same dataset (Chapman, 2012). In this study, we noticed that this problem is severe in small crater counts. For example, the crater floor of Tycho is covered by numerous fractures, low-relief mountains, and boulders. Small craters are hard to discern on these surfaces. Previous study (Hiesinger et al., 2010) counted ~3600 craters for a surface smaller than 1 km^2 in the crater floor. We did not include the crater floor in our counts because fracture pits and other depressions cannot be precisely distinguished from impact craters. For comparison, we counted ~2800 craters on a relatively flat impact melt pool ~1 km^2 (Appendix Table A.2; the "NE crater rim IMP 1" in Fig. 6). The subjective recognition of impact craters may significantly bias the results of small crater counts by different crater counters, especially at chaotic terrains.

This effect is more profound when counting the small crater populations on old surfaces, such as the counting areas in Mare Nubium and Alphonsus. Old surfaces may have gone through complicated resurfacing events. Although without complex topography, old craters smaller than 1 km diameter having obscure remnant rims may be included in one case but may be ruled out in another. For example, ~1130 craters were included in the LROC counts for the West Crater Floor (~0.31 km^2; Appendix Table A.1); ~1260 craters were counted in LROC images in a smaller counting area at the DHC 9 (~0.28 km^2; Appendix Table A.1). The crater floor of Alphonsus is older than the dark haloed craters but the number of the counted craters is ~19% less. Remnant rims of craters at older surfaces may bias a counter's judgment in choosing which craters to count. This effect is hard to completely avoid. We suggest that small crater counts should be performed with great cautious, especially at old surfaces.

5. Conclusion

We counted the small crater populations on both young and old lunar surfaces to determine the problems of using small crater counts for age dating. Our counting areas are not smaller than those used in other publications, and the absolute model ages were determined from the widely employed production and chronology functions. Great discrepancies are observed in the small crater counts.

The problems found in the small crater counts are summarized as the following:

1. For a same counting area, the crater densities, model ages, and size–frequency distribution curves in its two different diameter ranges are different.
2. For same-aged terrains, their crater densities, model ages, and size–frequency distribution curves are different from each other.

The small crater populations in the counting areas are possibly dominated by secondaries. Their nonuniform distribution and density in different surfaces and different diameter ranges may cause great uncertainties in age dating. This work shows that the size–frequency distributions of the potential small lunar and martian primaries ($D < 1$ km) are the same as that of the Population 2 craters on the inner Solar System bodies. Impactors forming secondaries have steep slopes and the observed steep upturns in crater size–frequency distributions at small diameter ranges are most likely to be caused by secondaries, not primaries. Small distant secondaries and primaries are hard to be firmly distinguished rendering small crater counts problematic. Small crater counts are highly unreliable for either relative or absolute age dating on both old and young surfaces. As shown in Figs. 5 and 8, for a same counting area, its absolute model ages in different diameter ranges may be significantly different from each other, and they do not reflect the real surface ages (i.e., Tycho has a possible sample age of ~ 109 Ma).

In general, statistics of small craters are affected by numerous factors, e.g., contamination of secondaries and different target properties. Crater counting is a subjective process which causes more uncertainties to the results. Simplistic attempts to date planetary surfaces from small crater counts may be invalidate if they do not take these factors into account.

To better understand the behavior of the size–frequency distributions of the secondaries populations, future work will focus on their crater equilibrium density and the roll-over diameter of their steeply-sloped size–frequency distribution curves.

Acknowledgments

We sincerely thank Drs. Clark R. Chapman and Beau Bierhaus for reviewing this paper and the insightful comments. Their great comments and suggestions helped us better understand the possible reasons for the observed problems in the small crater counts. Drs. Alfred McEwen and Gwendolyn D. Bart kindly provided their crater counts data. We thank Dr. Tomokatsu Morota for sharing the method in calibrating the Kaguya images.

Appendix Supplementary material

Supplementary data associated with this article can be found, in the online version, at http://dx.doi.org/10.1016/j.icarus.2012.05.012.

References

Arvidson, R. et al., 1979. Standard techniques for presentation and analysis of crater size–frequency data. Icarus 37, 467–474.
Ashworth, D.G., 1978. Lunar and planetary impact erosion. In: McDonnell, J.A.M. (Ed.), Cosmic Dust. Wiley, Hoboken, N.J., pp. 427–526.
Bart, G.D., Melosh, H.J., 2007. Using lunar boulders to distinguish primary from distant secondary impact craters. Geophys. Res. Lett. 34, L07203.
Bierhaus, E.B., Chapman, C.R., Merline, W.J., 2005. Secondary craters on Europa and implications for cratered surfaces. Nature 437, 1125–1127.
Bottke, W. F., Morbidelli, A., 2006. The asteroid and comet impact flux in the terrestrial planet region: A brief history of the last 4.6 Gy. In: 2006 Planetary Chronology Workshop. Abstract 6019.
Bottke, W.F., Nesvorny, D., Durda, D.D., 2005. Are most small craters primaries or secondaries: Insights from asteroid collisional/dynamical evolution models. Lunar Planet. Sci. XXXVI. Abstract 1489.
Bugiolacchi, R., Spudis, P.D., Guest, J.E., 2006. Stratigraphy and composition of lava flows in Mare Nubium and Mare Cognitum. Meteorit. Planet. Sci. 41 (2), 285–304.
Chapman, C.R., 2004. Mars cratering issues: Secondary cratering and end-Noachian degradation. In: Second Conference on Early Mars: Geologic, Hydrologic, and Climatic Evolution and the Implications for Life. Abstract 8028.
Chapman, C.R., 2012. Assessment of evidence for two populations of impactors in the inner Solar System: implications for terrestrial planetary body history. In: Microsymposium 53: Early History of the Terrestrial Planets: New Insights from the Moon and Mercury, March 17-18, Houston, TX.

Coombs, C.R., Hawke, B.R., Lucey, P.G., Owensby, P.D., Zisk, S.H., 1990. The Alphonsus region: a geologic and remote-sensing perspective. Proc. Lunar Planet. Sci. Conf. 20, 161–174.
Dundas, C.M., McEwen, A.S., 2007. Rays and secondary craters of Tycho. Icarus 186, 31–40.
Gault, D.E., 1970. Saturation and equilibrium conditions for impact cratering on the lunar surface. Criteria and implications. Radio Sci. 5 (2), 273–291.
Hartmann, W.K., 1970. Lunar cratering chronology. Icarus 13, 209–301.
Hartmann, W.K., 1984. Does crater 'saturation equilibrium' occur in the Solar System? Icarus 60, 56–74.
Hartmann, W.K., 2005. Martian cratering. 8. Isochron refinement and the history of martian geologic activity. Icarus 174, 294–320.
Hartmann, W.K., 2007. Martian cratering. 9. Toward resolution of the controversy about small craters. Icarus 189, 274–278.
Hartmann, W.K., Neukum, G., 2001. Cratering chronology and the evolution of Mars. Space Sci. Rev. 96, 165–194.
Hartmann, W.K., Neukum, G., Werner, S., 2008. Confirmation and utilization of the "production function" size–frequency distributions of martian impact craters. Geophys. Res. Lett. 35, L02205. http://dx.doi.org/10.1029/2007GL031557.
Hartung, J.B., 1976. Was the formation of a 20-km diameter impact crater on the moon observed on June 18, 1178? Meteoritics 11 (3), 187–194.
Hawke, B.R., Blewett, D.T., Lucey, P.G., Smith, G.A., Bell III, J.F., Campbell, B.A., Robinson, M.S., 2004. The origin of lunar crater rays. Icarus 170 (1), 1–16.
Head III J.W., Wilson, L., 1979. Alphonsus-type dark-halo craters: Morphology, morphometry and eruption conditions. Proc. Lunar Planet Sci. Conf. 10, 2861–2897.
Hiesinger, H., Head III, J.W., Jaumann, W.U., Neukum, G., 2003. Ages and stratigraphy of mare basalts in Oceanus Procellarum, Mare Nubium, Mare Cognitum, and Mare Insularum. J. Geophys. Res. (Planets) 108 (E7), 1–27. http://dx.doi.org/10.1029/2002JE001985.
Hiesinger, H., van der Bogert, C.H., Robinson, M.S., Klemm, K., Reiss, D., the LROC Team, 2010. New crater size–frequency distribution measurements for Tycho crater based on lunar reconnaissance orbiter camera images. Lunar Planet. Sci. XXXXI. Abstract 2287.
Hiesinger, H. et al., 2012. How old are young lunar craters? J. Geophys. Res. 117, E00H10. http://dx.doi.org/10.1029/2011JE003935.
Ivanov, B.A., 2001. Mars/Moon cratering rate ratio estimates. Space Sci. Rev. 96, 87–104.
Ivanov, B.A., 2006. Earth/Moon impact rate comparison: Searching constraints for lunar secondary/primary cratering proportion. Icarus 183 (2), 504–507.
Kato, M., Sasaki, S., Tanaka, K., Iijima, Y., Takizawa, Y., 2008. The Japanese lunar mission SELENE: Science goals and present status. Adv. Space Res. 42, 294–300.
McEwen, A.S., Bierhaus, E.B., 2006. The importance of secondary cratering to age constraints on planetary surfaces. Annu. Rev. Earth Planet. Sci. 34, 540–567.
McEwen, A.S. et al., 2005. The rayed crater Zunil and interpretations of small impact craters on Mars. Icarus 176, 351–381.
Melosh, H.J., 1989. Impact Cratering: A Geologic Process. Oxford Univ. Press, New York, pp. 1–255.
Michael, G.G., Neukum, G., 2010. Planetary surface dating from crater size–frequency distribution measurements: partial resurfacing events and statistical age uncertainty. Earth Planet. Sci. Lett. 294, 223–229.
Morota, T. et al., 2009. Formation age of the lunar crater Giordano Bruno. Meteorit. Planet. Sci. 44, 1115–1120.
Neukum, G., Ivanov, B.A., 1994. Crater size distributions and impact probabilities on Earth from lunar, terrestrial-planet, and asteroid cratering data. In: Gehrels, T. (Ed.), Hazards due to Comets and Asteroids. Univ. of Arizona Press, Tucson, pp. 359–416.
Neukum, G., Ivanov, B.A., Hartmann, W.K., 2001. Cratering records in the inner Solar System in relation to the lunar reference system. Space Sci. Rev. 96, 55–86.
Neukum, G., Wagner, R.J., Wolf, U., Denk, T., 2006. The cratering record and cratering chronologies of the saturnian satellites and the origin of impactors: Results from Cassini ISS Data. Euro. Planet. Sci. Conf. 2006-A-00610.
Ostrach, L.R., Robinson, M.S., Denevi, B.W., Thomas, P.C., 2011. Effects of incidence angle on crater counting observations. Lunar Planet Sci. Conf. XXXXII. Abstract 1202.
Plescia, J.B., Robinson, M.S., 2011. New constraints on the absolute lunar crater chronology. Lunar Planet. Sci. XXXXII. Abstract 1839.
Plescia, J.B., Robinson, M.S., Paige, D.A., 2010. Giordano Bruno: The young and the restless. Lunar Planet. Sci. Conf. XXXXI. Abstract 2038.
Richardson, J.E., 2009. Cratering saturation and equilibrium: A new model looks at an old problem. Icarus 204, 697–715.
Robinson, M.S. et al., 2005. LROC – Lunar Reconnaissance Orbiter Camera. Lunar Planet. Sci. XXXVI. Abstract 1576.
Schmedemann, N. et al., 2012. Crater Size–frequency Distribution (CSFD) and Chronology of Vesta – Crater Counts Matching HED Ages. Lunar Planet. Sci. XXXXIII. Abstract 2554.
Shoemaker, E.M., 1962. Interpretation of lunar craters. In: Kopal, Z. (Ed.), Physics and Astronomy of the Moon. Academic Press, New York, London, pp. 283–359.
Shoemaker, E.M., 1965. Preliminary analysis of the fine structure of the lunar surface in Mare Cognitum. In: Ranger 7, Part 2, Experimenters' Analyses and Interpretations. JPL/NASA Technical Report 32-700, pp. 75–134.
Shoemaker, E.M., Hackman, R.J., Eggleton, R.E., 1962. Interplanetary correlation of geologic time. Adv. Astronaut. Sci. 8, 70–89.
Shoemaker, E.M. et al., 1969. Television observations from Surveyor. In: Surveyor Program Results. U.S. Natl. Aeronautics Space Admin. Spec. Publ. SP-184, 19–128.
Smith, M.R., Gillespie, A.R., Montgomery, D.R., 2008. Effect of obliteration on crater-count chronologies for martian surfaces. J. Geophys. Res. 35, L10202.
Stoffer, D., Ryder, G., 2001. Stratigraphy and isotope ages of lunar geologic units: chronological standard for the inner Solar System. Space Sci. Rev. 96, 9–54.
Strom, R.G., Malhotra, R., Ito, T., Yoshida, F., Kring, D.A., 2005. The origin of planetary impactors in the inner Solar System. Science 309, 1847–1850.
Strom, R.G., Chapman, C.R., Merline, W.J., Solomon, S.J., Head III, J.W., 2008. Mercury cratering record viewed from MESSENGER's first flyby. Science 321, 79–81.
van der Bogert, C.H. et al., 2010. Discrepancies between crater size–frequency distributions on ejecta and impact melt pools at lunar craters: An effect of differing target properties? Lunar Planet. Sci. XXXXI. Abstract 2165.
Werner, S.C., van Gesselt, S., Neukum, G., 2003. Continual geological activity in Athabasca Valles, Mars. J. Geophys. Res. 108. http://dx.doi.org/10.1029/2002JE002020, ROV 22-1.
Werner, S.C., Ivanov, B.A., Neukum, G., 2009. Theoretical analysis of secondary cratering on Mars and an image-based study on the Cerberus Plains. Icarus 200, 406–417.
Wilcox, B.B., Robinson, M.S., Thomas, P.C., Hawke, B.R., 2005. Constraints on 829 the depth and variability of the lunar regolith. Meteorit. Planet. Sci. 40 (695–710), 830. http://dx.doi.org/10.1111/j.1945-5100.2005.tb00974.x.
Zanetti M., Hiesinger, H., Bogert, C.H., Reiss, D., Jolliff, B.L., 2012. Aristarchus crater: Mapping of impact melt and absolute age determination. Lunar Planet. Sci. XXXXII. Abstract 2330.
Zisk, S.H., Campbell, B.C., Pettengill, G.H., Brockelman, R., 1991. Alphonsus crater: Floor fracture and dark-mantle deposit distribution from new 3.0-cm radar images. Geophys. Res. Lett. 18 (11), 2137–2140.